Controllable ferroelectricity and bulk photovoltaic effect in elemental group-V monolayers through strain engineering

Fuming Xu [1], Hongjie Su,[1] Zhirui Gong,[1,*] Yadong Wei [1], Hao Jin [1,†] and Hong Guo[1,2]

[1]*College of Physics and Optoelectronic Engineering, Shenzhen University, Shenzhen 518060, China*
[2]*Centre for the Physics of Materials and Department of Physics, McGill University, Montréal, Canada H3A 2T8*

In this paper, based on the first-principles calculation combined with a $k \cdot p$ model, we systematically study the ferroelectricity and bulk photovoltaic effect (BPVE) in elemental group-V monolayers. Our results indicate that the electric polarization in group-V monolayers can be effectively tuned by external uniaxial strain, showing a perfect linear relationship. In addition, the Berry curvature and BPVE are well correlated to spontaneous polarizations, which are dominated by structural distortion. Remarkably, a quadratic relation between the shift current and the spontaneous polarization is observed in group-V monolayers. Accordingly, by manipulating the structural distortion through strain engineering, the BPVE can be generated in a controllable manner. Our work not only establishes the polarization-dependent BPVE in ferroelectric materials, but also paves the way for the development of BPVE-based ferroelectric devices.

I. INTRODUCTION

The bulk photovoltaic effect (BPVE) is a second-order nonlinear optical effect, which can occur in materials without external bias or *p-n* junctions [1–4]. In ferroelectric materials, the primary contributor to the BPVE is the shift current, arising from the shift of photoexcited electrons in real space upon interband transitions [5,6]. In previous studies, the BPVE is mainly explored in three-dimensional (3D) ferroelectrics, which is often hampered by low efficiency [7–10]. Nevertheless, it is suggested that a larger BPVE would exist in low-dimensional materials due to the reduction of crystal symmetry [11]. Recently, two-dimensional (2D) ferroelectricity has been theoretically investigated and demonstrated by experiments [12–17]. In addition, it is also predicted that the emerging 2D ferroelectric materials could have a large shift current, making them critical candidates for ferroelectric and photovoltaic applications [18–20]. However, we should point out that the mentioned ferroelectric materials are all compounds, which consist of different elements. The BPVE in these binary or ternary ferroelectric materials can be influenced by many aspects, such as atomic and electronic compositions, chemical bonding, and lattice distortion. Consequently, it is rather difficult to establish a general relation between the electric polarization and BPVE [18]. Fortunately, a family of 2D elemental materials, group-V monolayers, have been successfully synthesized recently [21,22]. Moreover, the ferroelectricity in elemental monolayers is mainly induced by a structural distortion, enabling us to completely understand how the BPVE depends on the structure of ferroelectric materials.

II. RESULTS AND DISCUSSION

The most studied structure for group-V monolayers is 2D black phosphorus [23,24], which shows a layered orthorhombic structure with the point group D_{2h}. As listed in Table S2 of the Supplemental Material [25], this kind of system contains eight symmetry operations including a center of inversion, while for other group-V monolayers, such as As and Sb, their optimized structures become distorted due to reduced sp^3 hybridization [26,27]. The buckled structure has a C_{2v} point group, in which the inversion symmetry is broken. To quantify the geometric distortion, we employ two angles, namely θ_u and θ_l, which are defined as the relative rotation of orange-colored atoms upon their nearby gray-colored ones [see Fig. 1(a)]. In this paper, we first explore the transition barrier (E_B) as a function of the tilting angle based on first-principles calculations (see details in Sec. II of the Supplemental Material [25] and Refs. [28–37] therein). Since the structure prefers to stay in the so-called angle-covariant phase [12,26,38], we construct the phase transition path along the one-dimensional line, in which $\theta_l = \theta_u$. As shown in Fig. 1(b), there are two stable energy-degenerate structures, namely the ferroelectric (FE) phase ($\theta_u = \theta_l \approx 6°$) and FE′ phase ($\theta_u = \theta_l \approx -6°$), which are connected by a saddle point, i.e., paraelectric (PE) phase ($\theta_u = \theta_l = 0$). The calculated transition barriers for As and Sb monolayers are about 13 and 91 meV, respectively, which are much smaller than those of traditional ferroelectric materials, e.g., PbTiO$_3$ ($\sim$200 meV) [39].

To explore the ferroelectricity in group-V monolayers, we calculate the spontaneous polarization (P_S) using the modern Berry phase method [40,41]. At zero temperature, the predicted P_S is 0.42×10^{-10} and 0.79×10^{-10} C/m for As and Sb monolayers, respectively. Further analysis reveals that the electric polarization in group-V monolayers is dominated by
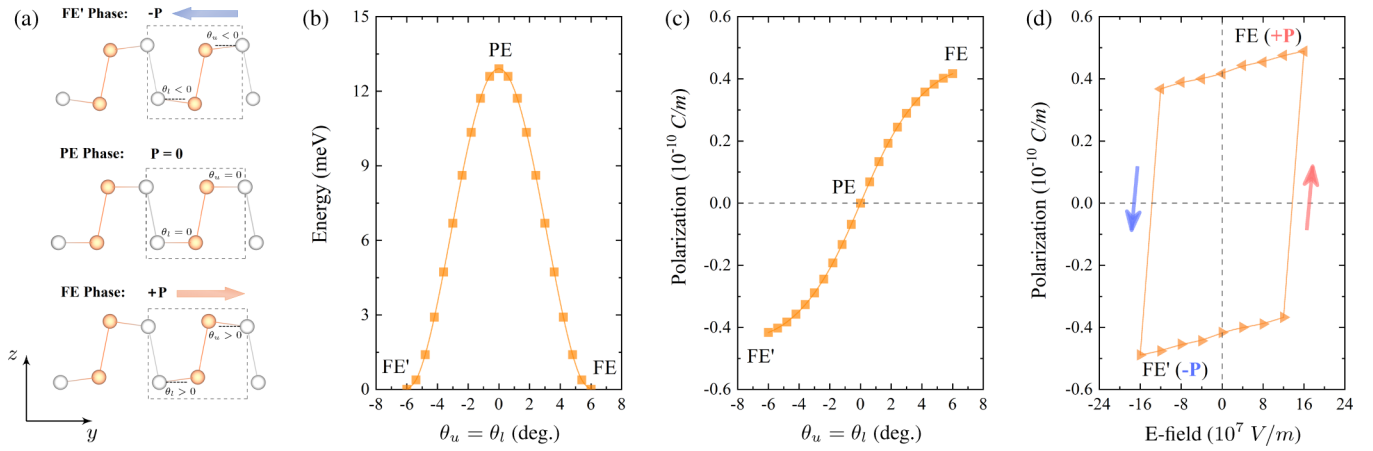
*gongzr@szu.edu.cn
†jh@szu.edu.cn

FIG. 1. (a) Side views of distorted (FE and FE′) and undistorted structures (PE). (b) Energy barrier and (c) electric polarization as a function of tilting angles ($\theta_l = \theta_u$) along the transition path for the As monolayer. (d) The polarization hysteresis loop in the As monolayer.

the in-plane y component of the electronic part, while the ionic contribution is zero (see Fig. S3 in the Supplemental Material [25]). In addition, from Fig. 1(c) we find that the FE and FE′ phases have opposite polarizing directions, which can be switched if the transition barrier is overcome. Based on the perturbation approach [42–44], we simulate the polarization hysteresis loop for the As monolayer (see details in Sec. IV B of the Supplemental Material [25] and Refs. [45–48] therein). As shown in Fig. 1(d), the critical electric field for the phase transition is 1.4×10^8 V/m, which is about 50% lower than the predicted value of PbTiO$_3$ [45]. In addition, we also study the ferroelectric Curie temperature by means of Monte Carlo (MC) simulations within the Landau-Ginzburg framework [25,49]. The fitted Curie temperature (T_C) is 225 K for the As monolayer, which is comparable to that of SnTe ($T_C =$ 270 K) and β-GeSe monolayers ($T_C =$ 212 K) [14,15,50], while for the Sb monolayer, due to the larger polarization and higher-energy barrier, the estimated T_C is up to 660 K. It is noticeable that the ferroelectricity in several 2D materials has been detected by using piezoresponse force microscopy (PFM) or scanning tunneling spectroscopy (STS) [15–17]. We thus expect that the robust ferroelectricity in group-V monolayers can be validated by similar techniques in the near future.

Since the ferroelectricity in elemental group-V monolayers is dominated by a geometric structure, it is of scientific importance to understand the influence of the structural distortion on the ferroelectric phase transition. To this end, we employ the strain engineering approach to precisely manipulate the structure buckling. Here, the uniaxial strain ε is defined as $\varepsilon = \Delta l / l$, where l is the equilibrium lattice constant and Δl is the deformation of l. In Figs. 2(a) and 2(b), we plot the in-plane spontaneous polarization and energy barrier of the As monolayer as a function of uniaxial strain. We find that both P_S and E_B are enhanced under compressive strain while decreased if tensile strain is applied. In addition, the in-plane spontaneous polarization shows a linear dependence on uniaxial strain. Within $\pm 2\%$ uniaxial strain along the x (y) direction, P_S could linearly change by about 20% (40%). Compared with P_S, E_B is more sensitive to the strain, especially along the y direction. This is because the As monolayer possesses extraordinary

flexibility, which exhibits a sensitive structural response to external strain (see details in Sec. III of the Supplemental Material [25] and Refs. [51–54] therein). To further explore the strain effect on the phase transition, we predict T_C under different strains along the y direction. Similar with E_B, T_C exhibits a quadratic behavior in terms of ε [see Fig. 2(c)]. It is worth noting that T_C could exceed room temperature when a small amount of compressive strain is applied, and reaches 532 K under 2% compressive strain. These results indicate that the ferroelectricity in group-V monolayers can be effectively manipulated by the application of strain engineering.

In Fig. 3(a), we plot the band structure of the As monolayer based on its orbital characteristics, in which the green, blue, and red colors represent p_x, p_y, and p_z orbitals of As atoms. Clearly, the monolayer As is a direct band-gap semiconductor, with the band edge position located at the point along the Y-Γ direction. At the Perdew-Burke-Ernzerhof (PBE) level, the calculated band gap is about 0.14 eV, which is much smaller than the value at the Γ point, i.e., 1.08 eV. To better estimate the band gap, we also perform calculations using the revised Heyd-Scuseria-Ernzerhof screened hybrid functional (HSE06) method [55,56]. As shown in Fig. S6 of the Supplemental Material [25], the band gap is significantly increased, with a value up to 0.60 eV. Nevertheless, the band dispersion maintains the same trend as that of the PBE calculations. It is also interesting to note that both the valence band maximum (VBM) and conduction band minimum (CBM) are dominated by the p_y orbital. To gain further insight into the effect of polarization on orbital characteristics, we plot band-decomposed charge densities of CBM and VBM for different phases. The results shown in Fig. 3(b) demonstrate that for the PE phase, due to its centrosymmetric nature, the charge density distribution exhibits highly symmetric behavior, and each As atom contributes equally to the CBM and VBM, while for the FE and FE′ phases, the VBM and CBM are contributed by different As atoms. This is especially beneficial for optical applications, since the photoexcited electron and hole are spatially separated, leading to relatively low recombinations [57,58]. Moreover, when the polarization is opposite, the charge density of each As atom also reverses its contributions to the VBM and CBM.
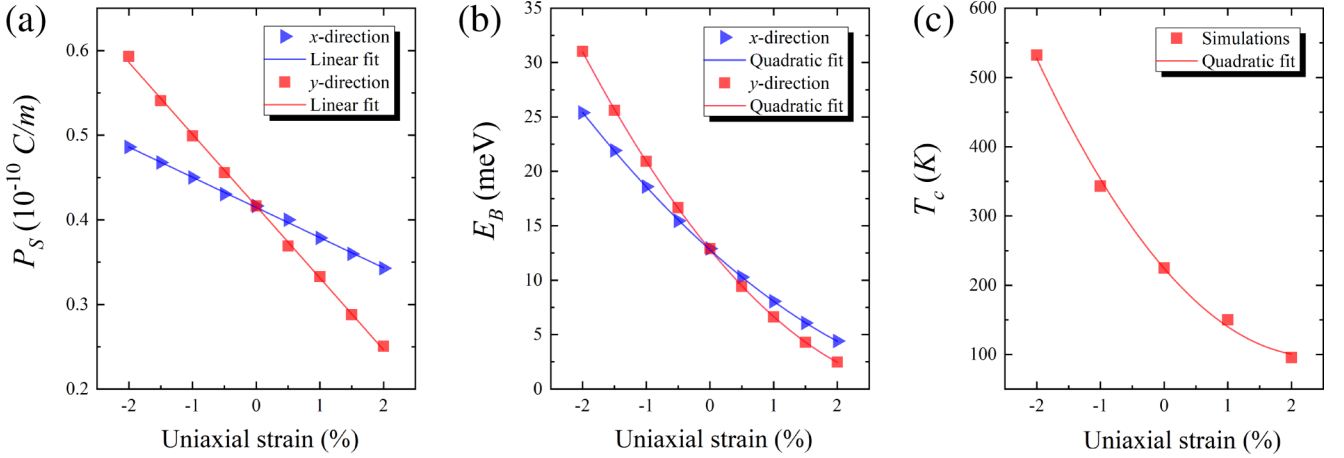
FIG. 2. (a) Spontaneous in-plane polarization (P_S), (b) energy barrier (E_B), and (c) ferroelectric Curie temperature (T_C) as a function of uniaxial strain (ε) in the As monolayer.

In the PE phase, the Berry curvature $\Omega(\boldsymbol{k})$ is zero due to the presence of time-reversal and inversion symmetries, while in the FE or FE' phase, the inversion symmetry is broken by electric polarization, resulting in a unique distribution of $\Omega(\boldsymbol{k})$. To elucidate the polarization-dependent distribution of the Berry curvature, we calculate $\Omega(\boldsymbol{k})$ in the first Brillouin zone, which is given by

$$\Omega_{n\mathbf{k},z} = 2i \sum_{m \neq n} \frac{\langle n|\partial \hat{H}/\partial k_x|m\rangle \langle m|\partial \hat{H}/\partial k_y|n\rangle}{\left(\epsilon_{\mathbf{k}}^n - \epsilon_{\mathbf{k}}^m\right)^2}, \qquad (1)$$

where $|n\rangle$ refers to the eigenstate in band n with eigenvalue $\epsilon_{\mathbf{k}}^n$ for a given momentum $\boldsymbol{k}$. Since $\Omega(\boldsymbol{k})$ varies rapidly, we take the logarithmic form of $\Omega(\boldsymbol{k})$ to ensure the rapid variation of the Berry curvature more visually [59]. As shown in Fig. 3(c), large Berry curvature peaks emerge at the band edge positions. Due to the time-reversal and $\mathcal{M}_x$ mirror symmetries, $\Omega(-\boldsymbol{k}) = -\Omega(\boldsymbol{k})$ and $\Omega(k_x, k_y) = -\Omega(-k_x, k_y)$. As a result, a pair of negative and positive Berry curvature peaks appear, resulting in a finite Berry curvature dipole [60,61].

Since the ferroelectricity can be manipulated via strain engineering, we also study the Berry curvature distribution under various strains. As shown in Fig. S8 of the Supplemental Material [25], $\Omega(\boldsymbol{k})$ is significantly enhanced under compressive strain, while it becomes much smaller if tensile strain is applied. Moreover, $\Omega(\boldsymbol{k})$ reverses the sign by polarization reversal. In this sense, the ferroelectricity provides an efficient way to generate large Berry curvatures in a controllable manner.

To shed light on the mechanism underlying the Berry curvature, we employ a $k \cdot p$ model to describe the As monolayer. The Hamiltonian can be expressed as

$$H = H_{kp} + H_{ep}. \qquad (2)$$

Here, H_{kp} describes the Hamiltonian without P_S, which is symmetric under the inversion transformation [24], while the second term H_{ep} is induced due to electric polarization, which plays an essential role in the emergence of the Berry curvature and the nonlinear optical response. By applying the second-order perturbation theory, we develop an effective
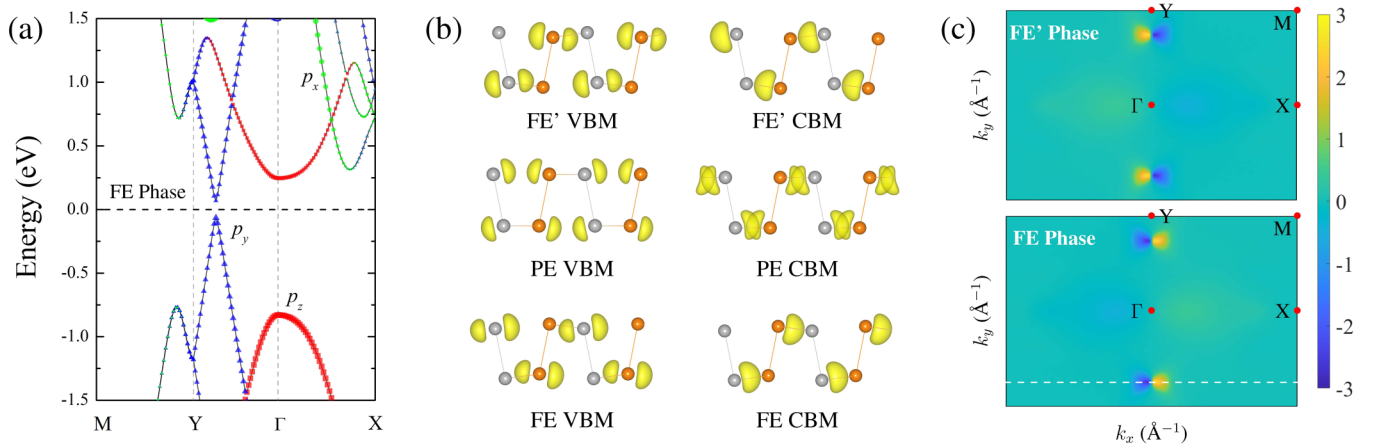

FIG. 3. (a) Orbit-projected band structure of the As monolayer, in which the green, blue, and red colors represent p_x, p_y, and p_z orbitals, respectively. The Fermi level is set to zero. (b) Band-decomposed charge densities of CBM and VBM for FE', PE, and FE phases. The isosurface value is set to 0.018 e/Å. (c) k-dependent distribution of Berry curvature at the Fermi energy level. Yellow and blue colors represent positive and negative contributions, respectively.
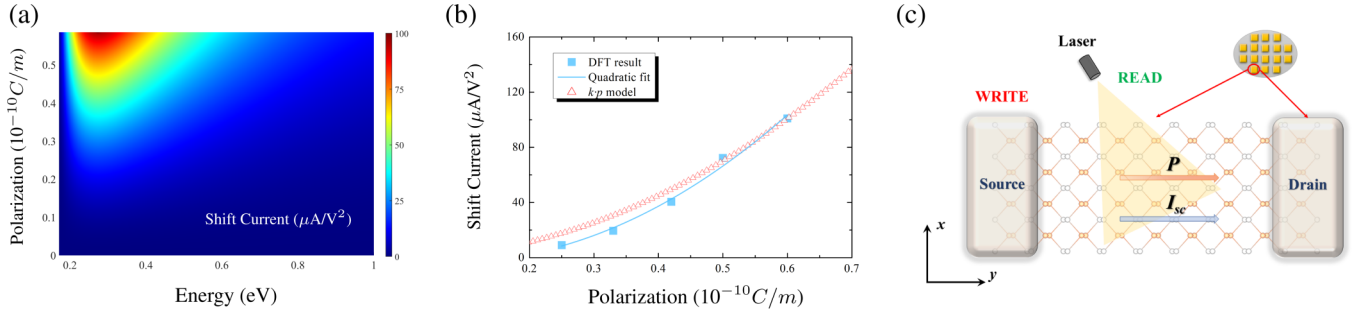
FIG. 4. (a) Calculated shift current spectra of the As monolayer. (b) The peaks of shift current as a function of polarization. (c) The schematic diagram of the proposed nonvolatile memory based on the ferroelectric group-V monolayer.

Hamiltonian (see Sec. VI of the Supplemental Material for details [25]), given as

$$H_{\text{eff}} = \epsilon_+(\boldsymbol{k})I_2 + \epsilon_-(\boldsymbol{k})\sigma_z + \delta k^2 l^2 \sigma_x - \Delta k_y l \sigma_y, \quad (3)$$

where $\epsilon_\pm$ are related to eigenvalues of the conduction and valence bands. l is related to the lattice constant, I_2 is a 2×2 identity matrix, and σ_i ($i = x, y, z$) are Pauli matrices. Here, δ and Δ are coupling constants, both of which are determined by structural distortion. When the structural distortion is small, the electric polarization has a linear relation with the structural distortion. Accordingly, it is reasonable to assume that the coupling constants are also proportional to P, i.e., $\Delta \approx \delta \propto P$. In Fig. S9 of the Supplemental Material [25], we plot the Berry curvature in terms of the coupling constant Δ. Clearly, $\Omega(\boldsymbol{k})$ is significantly enhanced with an increase of Δ, and reverses its sign if Δ becomes negative, which agrees well with our first-principles calculations. Further analysis reveals that both the Berry curvature and its dipole satisfy the quadratic relation of the polarization, consistent with our numerical calculations.

To quantify the nonlinear optical response in group-V monolayers, we calculate the shift current (J_{sc}^a), which is obtained based on the following expression [1,62],

$$J_{\text{sc}}^a = 2\sigma^{abc}(0; \omega, -\omega)\text{Re}[E^b(\omega)E^c(-\omega)], \quad (4)$$

where a, b, and c indices denote Cartesian directions. For linearly polarized incident light, $b = c$. The shift current conductivity $\sigma^{abb}(0; \omega, -\omega)$ is then expressed as [63]

$$\sigma^{abb}(0; \omega, -\omega) = -\frac{i\pi e^3}{\hbar^2} \int_{BZ} \frac{d\boldsymbol{k}}{(2\pi)^2} \sum_{n,m} f_{nm}$$

$$\times r_{mn}^b r_{nm}^{b;a} \delta(\omega_{mn} - \omega). \quad (5)$$

Here, $\hbar\omega_{nm} = E_n - E_m$ represents the energy difference between different bands. $f_{nm} = f_n - f_m$ is the difference of Fermi occupations. r_{mn}^b and $r_{nm}^{b;a}$ are written as

$$r_{mn}^b = (1 - \delta_{mn})A_{mn}^b,$$

$$r_{nm}^{b;a} = \partial_{k_a} r_{nm}^b - i(A_{nn}^a - A_{mm}^a)r_{nm}^b, \quad (6)$$

where $A_{mn}^b = i\langle m|\partial_{k_b}n\rangle$ is the Berry connection. Note that σ^{abc} is a tensor, so we only show the largest in-plane component, i.e., σ^{yxx}. As shown in Fig. 4(a), the calculated shift current spectra have peaks in the infrared light region due to the small band gap. In addition, the maximum value is up to 100 $\mu A/V^2$, which is much larger than that of traditional

ferroelectric materials, such as BiFeO$_3$ (0.05 $\mu A/V^2$) and BiTiO$_3$ (5 $\mu A/V^2$) [5,64]. Accordingly, the BPVE in 2D group-V monolayers is considerably large, making it a promising platform to explore the corresponding nonlinear optical effect.

To gain further insight on the nature of polarization-dependent BPVE, we calculate the peaks of the shift current as a function of P. The results are shown in Fig. 4(b). Remarkably, the shift current exhibits a quadratic behavior in terms of P, suggesting that by manipulating the polarization in ferroelectric group-V monolayers, the shift current can be precisely controlled. These results are further analyzed by our $k \cdot p$ model. As illustrated in Sec. VIII of the Supplemental Material [25], the leading terms of the shift current conductivity (σ^{yxx}) are determined by

$$\sigma^{yxx}(0; \omega, -\omega) \sim |r_{-+}^x|^2 R_{nm}^{y,x}, \quad (7)$$

where r_{-+}^x and $R_{nm}^{y,x}$ are the velocity matrix element and shift vector, respectively. Based on the linear relationship between coupling constants and electric polarization, the modulus of the velocity matrix element ($|r_{-+}^x|$) is proportional to P while the shift vector ($R_{nm}^{y,x}$) is independent of P [see Eq. (S12) and Eqs. (S20)– (S22) in the Supplemental Material]. As a result, $\sigma^{yxx}(0; \omega, -\omega)$ should show the quadratic relation of the electric polarization P, in agreement with our first-principles calculations. This intrinsic property makes group-V monolayers superior and can be exploited as a basic building block in a programmable nonvolatile memory. As illustrated in Fig. 4(c), the electric polarization in each unit could be positive or negative depending on the applied bias, which represents "0" or "1." In this case, the data are written into the device. Note that the data are recorded even when the power is removed. On the other hand, if the device is illuminated by infrared light, a large BPVE occurs in the device, in which the shift current flows from the drain to source or vice versa depending on the polarization. In this case, the data are read from the device. Unlike traditional ferroelectric nonvolatile memory, this nanodevice exhibits a particular advantage in the read-out operation, which avoids the destructive process [65,66].

III. CONCLUSIONS

In summary, based on first-principles calculations, we have demonstrated that in-plane spontaneous polarization in group-V monolayers is induced by a structural distortion. Within ±2% uniaxial strain along the x or y direction, electric polar-

ization could linearly change by about 20% or 40%. Through MC simulations, we estimate the Curie temperatures, which can be increased quickly by applying a compressive strain. In addition, the BPVE in group-V monolayers is explored in detail. The results show that the As monolayer has a large shift current, with a value up to 100 μA/V^2. Further analysis based on the $k \cdot p$ model reveals that the shift current is well correlated to spontaneous polarization, which exhibits a quadratic behavior in terms of electric polarization. Based on these results, a nonvolatile memory with a nondestructive read-out operation is put forward. Thus, our work gives insight into how the BPVE can be controlled through strain engineering, which opens a way to the design of advanced nanodevices for ferroelectric and photovoltaic applications.

ACKNOWLEDGMENT

[1] J. E. Sipe and A. I. Shkrebtii, Phys. Rev. B **61**, 5337 (2000).

[2] F. Wang, S. M. Young, F. Zheng, I. Grinberg, and A. M. Rappe, Nat. Commun. **7**, 10419 (2016).

[3] D. E. Parker, T. Morimoto, J. Orenstein, and J. E. Moore, Phys. Rev. B **99**, 045121 (2019).

[4] M. M. Seyfouri and D. Wang, Crit. Rev. Solid State Mater. Sci. **46**, 83 (2021).

[5] S. M. Young and A. M. Rappe, Phys. Rev. Lett. **109**, 116601 (2012).

[6] L. Z. Tan and A. M. Rappe, Phys. Rev. Lett. **116**, 237402 (2016).

[7] S. Y. Yang, J. Seidel, S. J. Byrnes, P. Shafer, C.-H. Yang, M. D. Rossell, P. Yu, Y.-H. Chu, J. F. Scott, J. W. Ager, III, L. W. Martin, and R. Ramesh, Nat. Nanotechnol. **5**, 143 (2010).

[8] R. Nechache, C. Harnagea, S. Licoccia, E. Traversa, A. Ruediger, A. Pignolet, and F. Rosei, Appl. Phys. Lett. **98**, 202902 (2011).

[9] Z. Sun, X. Liu, T. Khan, C. Ji, M. A. Asghar, S. Zhao, L. Li, M. Hong, and J. Luo, Angew. Chem. Int. Ed. **55**, 6545 (2016).

[10] M. Nakamura, S. Horiuchi, F. Kagawa, N. Ogawa, T. Kurumaji, Y. Tokura, and M. Kawasaki, Nat. Commun. **8**, 281 (2017).

[11] Y. J. Zhang, T. Ideue, M. Onga, F. Qin, R. Suzuki, A. Zak, R. Tenne, J. H. Smet, and Y. Iwasa, Nature (London) **570**, 349 (2019).

[12] R. Fei, W. Kang, and L. Yang, Phys. Rev. Lett. **117**, 097601 (2016).

[13] M. Wu and X. C. Zeng, Nano Lett. **16**, 3236 (2016).

[14] W. Wan, C. Liu, W. Xiao, and Y. Yao, Appl. Phys. Lett. **111**, 132904 (2017).

[15] K. Chang, J. Liu, H. Lin, N. Wang, K. Zhao, A. Zhang, F. Jin, Y. Zhong, X. Hu, W. Duan, Q. Zhang, L. Fu, Q.-K. Xue, X. Chen, and S.-H. Ji, Science **353**, 274 (2016).

[16] M. Si, P.-Y. Liao, G. Qiu, Y. Duan, and P. D. Ye, ACS Nano **12**, 6700 (2018).

[17] K. Yasuda, X. Wang, K. Watanabe, T. Taniguchi, and P. Jarillo-Herrero, Science **372**, 1458 (2021).

[18] T. Rangel, B. M. Fregoso, B. S. Mendoza, T. Morimoto, J. E. Moore, and J. B. Neaton, Phys. Rev. Lett. **119**, 067402 (2017).

[19] R. P. Tiwari, B. Birajdar, and R. K. Ghosh, Phys. Rev. B **101**, 235448 (2020).

[20] J. Wei, Y. Li, L. Wang, W. Liao, B. Dong, C. Xu, C. Zhu, K.-W. Ang, C.-W. Qiu, and C. Lee, Nat. Commun. **11**, 6404 (2020).

[21] J. Shah, W. Wang, H. M. Sohail, and R. I. G. Uhrberg, 2D Mater. **7**, 025013 (2020).

[22] Z.-Q. Shi, H. Li, Q.-Q. Yuan, C.-L. Xue, Y.-J. Xu, Y.-Y. Lv, Z.-Y. Jia, Y. Chen, W. Zhu, and S.-C. Li, ACS Nano **14**, 16755 (2020).

[23] R. Fei, V. Tran, and L. Yang, Phys. Rev. B **91**, 195319 (2015).

[24] D. J. P. de Sousa, L. V. de Castro, D. R. da Costa, J. M. Pereira, and T. Low, Phys. Rev. B **96**, 155427 (2017).

[25] See Supplemental Material at http://link.aps.org/supplemental/10.1103/PhysRevB.106.195418 for computational details (Sec. I), lattice constants (Sec. II), elastic properties (Sec. III), ferroelectric properties (Sec. IV), band structures (Sec. V), explanation of the $k \cdot p$ model (Sec. VI), Berry curvature and its dipole (Sec. VII), and shift currents (Sec. VIII) for group-V monolayers.

[26] C. Xiao, F. Wang, S. A. Yang, Y. Lu, Y. Feng, and S. Zhang, Adv. Funct. Mater. **28**, 1707383 (2018).

[27] M. U. Rehman, C. Hua, and Y. Lu, Chin. Phys. B **29**, 057304 (2020).

[28] G. Kresse and J. Furthmüller, Comput. Mater. Sci. **6**, 15 (1996).

[29] G. Kresse and J. Furthmüller, Phys. Rev. B **54**, 11169 (1996).

[30] H. J. Monkhorst and J. D. Pack, Phys. Rev. B **13**, 5188 (1976).

[31] S. Grimme, J. Antony, S. Ehrlich, and H. Krieg, J. Chem. Phys. **132**, 154104 (2010).

[32] S. Grimme, S. Ehrlich, and L. Goerigk, J. Comput. Chem. **32**, 1456 (2011).

[33] G. Henkelman, B. P. Uberuaga, and H. Jónsson, J. Chem. Phys. **113**, 9901 (2000).

[34] P. Giannozzi, S. Baroni, N. Bonini, M. Calandra, R. Car, C. Cavazzoni, D. Ceresoli, G. L. Chiarotti, M. Cococcioni, I. Dabo, A. Dal Corso, S. de Gironcoli, S. Fabris, G. Fratesi, R. Gebauer, U. Gerstmann, C. Gougoussis, A. Kokalj, M. Lazzeri, L. Martin-Samos *et al.*, J. Phys.: Condens. Matter **21**, 395502 (2009).

[35] J. P. Perdew, K. Burke, and M. Ernzerhof, Phys. Rev. Lett. **77**, 3865 (1996).

[36] D. R. Hamann, Phys. Rev. B **88**, 085117 (2013).

[37] G. Pizzi, V. Vitale, R. Arita, S. Bluegel, F. Freimuth, G. Geranton, M. Gibertini, D. Gresch, C. Johnson, T. Koretsune, J. Ibanez-Azpiroz, H. Lee, J.-M. Lihm, D. Marchand, A. Marrazzo, Y. Mokrousov, J. I. Mustafa, Y. Nohara, Y. Nomura, L. Paulatto *et al.*, J. Phys.: Condens. Matter **32**, 165902 (2020).

[38] Y. Wang, C. Xiao, M. Chen, C. Hua, J. Zou, C. Wu, J. Jiang, S. A. Yang, Y. Lu, and W. Ji, Mater. Horiz. **5**, 521 (2018).

[39] R. E. Cohen, Nature (London) **358**, 136 (1992).

[40] R. D. King-Smith and D. Vanderbilt, Phys. Rev. B **47**, 1651 (1993).

[41] R. Resta, Rev. Mod. Phys. **66**, 899 (1994).

[42] R. W. Nunes and X. Gonze, Phys. Rev. B **63**, 155107 (2001).

[43] I. Souza, J. Íñiguez, and D. Vanderbilt, Phys. Rev. Lett. **89**, 117602 (2002).

[44] H. Fu and L. Bellaiche, Phys. Rev. Lett. **91**, 057601 (2003).

[45] C. Liu, Y. Chen, and C. Dames, Phys. Rev. Appl. **11**, 044002 (2019).

[46] C. Liu, V. Mishra, Y. Chen, and C. Dames, Adv. Theory Simul. **1**, 1800098 (2018).

[47] W. Ma and A. Hao, J. Appl. Phys. **115**, 104105 (2014).

[48] S. J. Ahmed, S. Pichardo, L. Curiel, and O. Rubel, Modell. Simul. Mater. Sci. Eng. **22**, 055014 (2014).

[49] R. A. Cowley, Adv. Phys. **29**, 1 (1980).

[50] S. Guan, C. Liu, Y. Lu, Y. Yao, and S. A. Yang, Phys. Rev. B **97**, 144104 (2018).

[51] E. Cadelano, P. L. Palla, S. Giordano, and L. Colombo, Phys. Rev. B **82**, 235414 (2010).

[52] A. Castellanos-Gomez, M. Poot, G. A. Steele, H. S. J. van der Zant, N. Agraït, and G. Rubio-Bollinger, Adv. Mater. **24**, 772 (2012).

[53] C. Lee, X. Wei, J. W. Kysar, and J. Hone, Science **321**, 385 (2008).

[54] Y. Ding, Y. Wang, L. Shi, Z. Xu, and J. Ni, Phys. Status Solidi RRL **8**, 939 (2014).

[55] J. Heyd, G. E. Scuseria, and M. Ernzerhof, J. Chem. Phys. **118**, 8207 (2003).

[56] A. V. Krukau, O. A. Vydrov, A. F. Izmaylov, and G. E. Scuseria, J. Chem. Phys. **125**, 224106 (2006).

[57] H. Jin, J. Li, B. Wang, Y. Yu, L. Wan, F. Xu, Y. Dai, Y. Wei, and H. Guo, J. Mater. Chem. C **4**, 11253 (2016).

[58] H. Jin, J. Li, Y. Wei, Y. Dai, and H. Guo, ACS Appl. Mater. Interfaces **10**, 25401 (2018).

[59] J. Li, H. Jin, Y. Wei, and H. Guo, Phys. Rev. B **103**, 125403 (2021).

[60] I. Sodemann and L. Fu, Phys. Rev. Lett. **115**, 216806 (2015).

[61] H. Jin, H. Su, X. Li, Y. Yu, H. Guo, and Y. Wei, Phys. Rev. B **104**, 195404 (2021).

[62] R. von Baltz and W. Kraut, Phys. Rev. B **23**, 5590 (1981).

[63] J. Ibañez-Azpiroz, S. S. Tsirkin, and I. Souza, Phys. Rev. B **97**, 245143 (2018).

[64] S. M. Young, F. Zheng, and A. M. Rappe, Phys. Rev. Lett. **109**, 236601 (2012).

[65] V. Garcia, S. Fusil, K. Bouzehouane, S. Enouz-Vedrenne, N. D. Mathur, A. Barthélémy, and M. Bibes, Nature (London) **460**, 81 (2009).

[66] R. C. G. Naber, K. Asadi, P. W. M. Blom, D. M. de Leeuw, and B. de Boer, Adv. Mater. **22**, 933 (2010).